

## Near Infrared Photometry of L and T Dwarfs

Denise C. Stephens<sup>1</sup>, Mark S. Marley<sup>2</sup>, Keith S. Noll<sup>3</sup>

### Abstract.

To better understand and model the atmospheres of L ( $T_{\text{eff}} \sim 2200$  K to 1400 K) and T ( $T_{\text{eff}} \lesssim 1300$  K) dwarfs, we've obtained  $K$ - and  $L$ -band photometry with the Keck I telescope for a representative sample. These observations were motivated in part by our desire to understand the abundance of  $\text{CH}_4$  and  $\text{H}_2\text{O}$  particularly at the L to T transition where CO reacts with  $\text{H}_2$  to produce these molecules. Here we present our most recent observations, discuss the trends we observe in color, and compare the Keck  $K$  and  $L'$  filters with the new Mauna Kea Observatory (MKO)  $K$  and  $L'$  filters.

### 1. Observations and Filter Selection

The data were obtained on April 13<sup>th</sup> and 14<sup>th</sup> UT 2000 using the Near Infrared Camera (NIRC) on the Keck I telescope at the W.M. Keck Observatory. Photometry was acquired using the  $K$ ,  $K_s$ ,  $L'$ , and  $L_s$  filters. These filters were selected due to their ability to identify the first appearance of methane ( $\text{CH}_4$ ) at  $3.3 \mu\text{m}$  and because of their sensitivity to the growth of the methane band at  $2.2 \mu\text{m}$  in the T dwarfs. We are interested in the appearance and strength of  $\text{CH}_4$  because chemical equilibrium favors  $\text{CH}_4$  over CO with falling atmospheric temperature (Fegley & Lodders 1996), thus the abundance of  $\text{CH}_4$  can be used as a constraint on the effective temperature of late L and T dwarfs.

In particular we are interested in the strong  $\nu_3$  fundamental band of  $\text{CH}_4$  at  $3.3 \mu\text{m}$  that is observable in some of the late L dwarfs (Noll et al. 2000) and all of the T dwarfs. The Keck  $L_s$  band overlaps this feature and can measure the strength of the absorption band while the Keck  $L'$  filter measures mostly continuum. This is seen in Figure 1 which shows spectra of the T dwarf Gliese 229B ( $\sim 950$  K) and the bandwidths for the Keck and MKO filters.

Table I lists the L and T dwarfs we observed, their coordinates, magnitudes and colors. The photometry was placed on a standard infrared system using the UKIRT IRCAM3 Fundamental and Extended list of standard stars (Hawarden et al. 2001). Note that this is not the same as the Mauna Kea Observatory (MKO) system which will be presented later. Since standard  $L'$  and  $L_s$  magnitudes are not available, we determined standard magnitudes for these bands by observing

---

<sup>1</sup>New Mexico State University

<sup>2</sup>Space Sciences Division/NASA Ames Research Center

<sup>3</sup>Space Telescope Science Institute

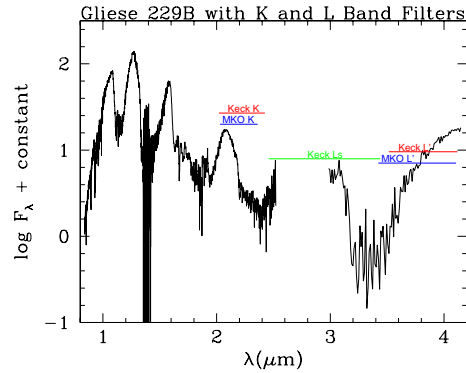


Figure 1. Spectra of Gliese 229B with the Keck  $K$ ,  $L_s$  and  $L'$  filters and the MKO  $K$  and  $L'$  filters. Note that the Keck  $L_s$  filter probes the appearance of methane at  $3.3 \mu\text{m}$  and that the MKO  $L'$  filter is also slightly sensitive to this absorption band.

only main sequence standard stars with spectral types between A0 V and G6 V, and then estimated a standard  $L'$  and  $L_s$  magnitude for each star using the intrinsic colors given by Bessell & Brett (1988) for main sequence stars.

## 2. Infrared Colors

Figure 2a presents the  $(K-L')$  color of our objects as a function of L and T dwarf spectral type. In general the  $(K-L')$  color gradually increases with later L- and T-dwarf spectral type. A linear least squares fit of the data to the L dwarf index shows that the  $(K-L')$  colors are reasonably well fit (correlation coefficient,  $r=0.8$ ). This increase in color is due to increasing molecular absorption in the  $K$  band. As  $T_{\text{eff}}$  decreases with later spectral type, the wings of the  $\text{H}_2\text{O}$  band at  $1.9 \mu\text{m}$  and pressure induced  $\text{H}_2 - \text{H}_2$  absorption together suppress the  $K$ -band flux. In the  $L'$  band the principle opacity source is  $\text{H}_2\text{O}$  alone. As the temperature decreases, the mean opacity source increases more slowly in the  $L'$  band than in the  $K$  band. The net result is that the total flux emitted in the  $K$  band falls faster than the total flux emitted in the  $L'$  band with decreasing temperature. This produces the redder  $(K-L')$  color with later L-dwarf spectral type.

A similar mechanism is responsible for the gradual reddening of the T dwarfs. For these objects  $\text{CH}_4$  at  $2.2 \mu\text{m}$  joins  $\text{H}_2\text{O}$  and  $\text{H}_2\text{-H}_2$  as the principal opacity sources in  $K$ . A linear least-squares fit ( $r=0.97$ ) of the T dwarf data produces a slightly steeper line. This change in slope from the L to T dwarfs suggests that the additional appearance of  $\text{CH}_4$  further suppresses the  $K$ -band flux, resulting in a steeper  $(K-L')$  color increase throughout the T dwarfs. Since the abundance of  $\text{CH}_4$  varies with  $T_{\text{eff}}$  and it is the dominant opacity source for T dwarfs in  $K$  band, but not  $L'$ , the  $(K-L')$  color should prove to be a good diagnostic for estimating  $T_{\text{eff}}$  for T dwarfs.

Figure 2b presents the  $(K-L_s)$  color of our objects as a function of L and T dwarf spectral type. Like the  $(K-L')$  color, the increase in  $(K-L_s)$  through the L

Table 1. Colors and Magnitudes of Target Objects

Object Name	Spec <sup>a</sup>	K mag	L' mag	L <sub>s</sub> mag	K-L'	K-L <sub>s</sub>
TVLM 513-46546	M8.5	10.74 ± 0.01	9.92 ± 0.05	10.57 ± 0.05	0.82 ± 0.06	0.17 ± 0.05
DENIS J1159384+005727	L0	12.80 ± 0.01	11.87 ± 0.05	12.60 ± 0.04	0.93 ± 0.05	0.20 ± 0.04
2MASSW J1035245+250745	L1	13.33 ± 0.02	12.56 ± 0.05	14.46 ± 0.06	0.78 ± 0.05	-1.12 ± 0.07
DENIS J1441373-094559	L1	12.66 ± 0.03	11.78 ± 0.06	13.74 ± 0.06	0.88 ± 0.07	-1.08 ± 0.07
2MASSW J1411175+393636	L1.5	13.25 ± 0.01	12.22 ± 0.04	13.08 ± 0.03	1.03 ± 0.04	0.17 ± 0.03
2MASSW J0928397-160312	L2	13.63 ± 0.03	12.72 ± 0.08	13.38 ± 0.06	0.91 ± 0.09	0.25 ± 0.07
2MASSW J1338261+414034	L2.5	12.73 ± 0.02	11.72 ± 0.05	12.49 ± 0.02	1.01 ± 0.05	0.24 ± 0.03
2MASSW J1615441+355900	L3	12.92 ± 0.02	11.61 ± 0.05	12.60 ± 0.05	1.31 ± 0.06	0.32 ± 0.06
2MASSW J1155009+230706	L4	14.07 ± 0.01	12.75 ± 0.05	13.70 ± 0.05	1.33 ± 0.05	0.38 ± 0.05
2MASSW J1246467+402715	L4	13.22 ± 0.02	11.88 ± 0.04	12.79 ± 0.03	1.33 ± 0.04	0.42 ± 0.03
2MASSW J1112257+354813	L4.5	12.69 ± 0.02	11.38 ± 0.03	12.28 ± 0.02	1.31 ± 0.04	0.41 ± 0.03
2MASSW J1328550+211449	L5	14.20 ± 0.01	13.01 ± 0.06	13.84 ± 0.06	1.20 ± 0.06	0.37 ± 0.06
2MASSW J1553214+210907	L5.5	14.67 ± 0.02	13.26 ± 0.07	13.93 ± 0.06	1.41 ± 0.07	0.74 ± 0.06
2MASSI J0756252+124456	L6	14.89 ± 0.02	13.33 ± 0.07	14.56 ± 0.05	1.55 ± 0.07	0.32 ± 0.06
2MASSW J0829570+265510	L6.5	14.87 ± 0.02	13.23 ± 0.07	14.18 ± 0.05	1.64 ± 0.07	0.68 ± 0.06
2MASSI J1526140+204341	L7	13.91 ± 0.01	12.59 ± 0.06	13.50 ± 0.05	1.32 ± 0.06	0.41 ± 0.05
2MASSI J0825196+211552	L7.5	13.02 ± 0.01	11.34 ± 0.04	12.43 ± 0.05	1.68 ± 0.04	0.59 ± 0.05
2MASSW J1632291+190441	L8	14.01 ± 0.01	12.58 ± 0.08	13.52 ± 0.05	1.43 ± 0.08	0.49 ± 0.05
SDSS 0837172-000018	T1	15.97 ± 0.04	14.42 ± 0.11	15.71 ± 0.09	1.54 ± 0.12	0.26 ± 0.10
SDSS 1254539-012247	T2	13.95 ± 0.01	12.12 ± 0.05	13.62 ± 0.04	1.83 ± 0.05	0.34 ± 0.05
SDSS 1021097-030420	T3	15.40 ± 0.03	13.53 ± 0.10	15.53 ± 0.08	1.86 ± 0.10	-0.13 ± 0.08
SDSS 1346465-003150	T6	15.89 ± 0.03	13.55 ± 0.06	15.56 ± 0.07	2.35 ± 0.07	0.34 ± 0.08
SDSS 1624144+002916	T6	15.66 ± 0.02	13.22 ± 0.06	15.43 ± 0.09	2.44 ± 0.07	0.24 ± 0.10

<sup>a</sup>Spectral Class: M and L from Kirkpatrick et al. (1999); T from Burgasser et al. (2001)

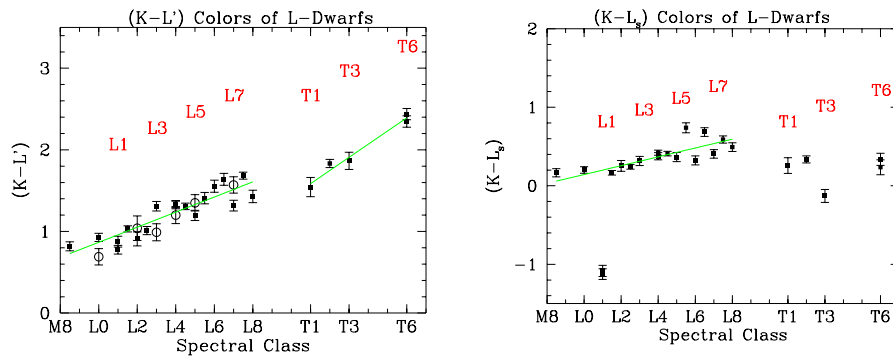


Figure 2.  $(K-L')$  and  $(K-L_s)$  colors as a function of spectral type. The squares represent data from Table 1, and the six open circles are L dwarfs taken from Leggett et al. (2001a).

dwarf sequence is due to increasing H<sub>2</sub>O and H<sub>2</sub>-H<sub>2</sub> absorption in the *K* band. A linear least squares fit applied to this data ( $r=0.5$ ) is shown. It is interesting to note that there appears to be substantially more scatter in the (*K-L<sub>s</sub>*) color for the later L dwarfs as compared with the early L dwarfs. This scatter may arise from differences in cloud cover (Gelino et al. 2001), or possibly atmospheric dynamics or metallicity producing greater variability in CH<sub>4</sub> abundance in these objects.

For the T dwarfs, CH<sub>4</sub> absorption definitely occurs both at 3.3  $\mu\text{m}$  and 2.2  $\mu\text{m}$ , which results in a suppression of the flux in the *L<sub>s</sub>* and *K* bands. Since the  $\nu_3$  fundamental band at 3.3  $\mu\text{m}$  is a factor of 100 times stronger than the  $\nu_2 + \nu_3$  combination band at 2.2  $\mu\text{m}$ , there is a greater suppression of the flux in the *L<sub>s</sub>* band than in the *K* band, which results in a bluer color for the T dwarfs. The break in (*K-L<sub>s</sub>*) color from the latest L dwarfs to the earliest T dwarfs suggests that perhaps very early T dwarfs, or very late L dwarfs have yet to be discovered, or that substantial CH<sub>4</sub> absorption appears rapidly over a very small T<sub>eff</sub> range.

Note that the two L1 dwarfs have very blue (*K-L<sub>s</sub>*) colors but unexceptional (*K-L'*) colors. These two objects were also unusually faint in narrow band 3.3  $\mu\text{m}$  images obtained the same night. This suggests that another opacity source is affecting the flux in the *L<sub>s</sub>* band for these two objects. Clearly 3-4  $\mu\text{m}$  spectroscopy of these objects is needed to constrain what is suppressing the flux in the *L<sub>s</sub>* band.

### 3. Comparison of the Keck Filters with the Mauna Kea Observatory (MKO) Filters

When comparing photometry obtained with different instruments it is necessary to understand that there is not a "standard" near-infrared photometric system. In an attempt to avoid water bands, observers have created near-infrared filters that are narrower than the original Johnson filters, all of which vary from one another in bandwidth and central wavelength location. Because no attempt has been made to regulate the size and location of near-infrared filters, the current filter sets used at observatories today bear very little resemblance to one another. This creates problems when trying to reproduce measurements at different observatories or when using standard star systems obtained from other telescopes. To make our research as valid as possible, we used the UKIRT Fundamental and Extended list of faint near infrared standard stars (Hawarden et al. 2001) to place our photometry on the UKIRT IRCAM3 system. We chose this system because the UKIRT *K* band filter most resembles the Keck *K* band filter as seen in figure 3a and when both filters are convolved with the spectra of main sequence stars; they produce almost identical *K* band magnitudes.

In an attempt to standardize near-infrared photometric passbands, the IAU Working Group on Infrared Photometry endorsed the Mauna Kea Observatory (MKO) near-infrared system as the preferred standard photometric system for near infrared photometry. These filters were designed to maximize throughput while minimizing the background and avoiding atmospheric water vapor. Since this filter set is now in use at UKIRT and many L and T dwarfs are being observed with this new filter set (Leggett et al. 2001b), it is valuable to compare

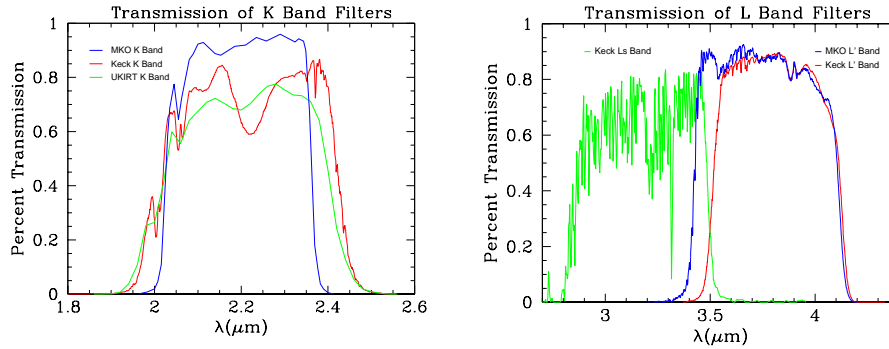


Figure 3.  $K$ - and  $L$ -band filter transmission curves for MKO, Keck and UKIRT. The MKO  $K$  filter is narrower and has much steeper sides than the Keck and UKIRT  $K$  filters which have similar profiles. In figure 3b the MKO  $L'$  filter extends farther into the blue by  $0.1 \mu\text{m}$  than the Keck  $L'$  filter.

the Keck magnitude and color results with predicted results using the MKO filters as done in Table 2. This table was created by convolving the atmospheric models of Marley et al. (2001) with the Keck  $K$  and  $L'$  filters, and the MKO  $K$  and  $L'$  filters to determine the typical magnitude that each of these filters would measure. The models used were for brown dwarfs ranging in effective temperature from 400 to 2000 K and approximately  $30 M_J$  in size.

It is clear from the table that the Keck  $K$  band magnitude is systematically fainter by 0.08 magnitude from the MKO  $K$  magnitude, and the larger difference seen in the T dwarfs is likely due to higher sensitivity of the Keck  $K$  band to the  $\text{CH}_4$  band at  $2.2 \mu\text{m}$ . Of greater interest is the difference in the  $L'$  magnitude for the two systems where the Keck  $L'$  magnitude is brighter by 10% and 20% for the late L and early T dwarfs. This difference occurs because the MKO filter extends  $0.1 \mu\text{m}$  farther into the blue and is consequently more sensitive to the appearance of the  $\text{CH}_4$  band at  $3.3 \mu\text{m}$  (See Figures 3b & 1). When we compare the colors produced by these systems, we find that there is a significant difference between the Keck and MKO ( $K-L'$ ) colors. Because the Keck ( $K-L'$ ) color is not as sensitive to the  $3.3 \mu\text{m}$   $\text{CH}_4$  band as the MKO ( $K-L'$ ) colors, the Keck ( $K-L'$ ) color serves as a better temperature diagnostic for the late L and early T dwarfs.

#### 4. Conclusions

We find that the ( $K-L'$ ) and ( $K-L_s$ ) colors become redder with later L dwarf spectral type. Similarly, the ( $K-L'$ ) color of the T dwarfs steadily reddens by a full magnitude over the range of objects observed, and this color may prove useful in the future classification and determination of effective temperature in T dwarfs. We find that slight differences in the bandwidths of the Keck and MKO filters are such that the Keck ( $K-L'$ ) color is always larger than the MKO ( $K-L'$ ) color and is a better indicator of effective temperature for the late L and T dwarfs because it is less affected by the strong  $\text{CH}_4$  absorption at  $3.3 \mu\text{m}$ .

Table 2. Keck and MKO Colors and Magnitudes

$T_{\text{eff}}$ (K)	$K_{KECK}$ (mag)	$K_{MKO}$ (mag)	$K_{K-}$ $K_M$	$L'_{KECK}$ (mag)	$L'_{MKO}$ (mag)	$L'_{K-}$ $L'_M$	Keck ( $K - L'$ )	MKO ( $K - L'$ )	$(K - L')_{K-}$ $(K - L')_M$
400	23.99	23.87	0.12	16.95	17.39	-0.44	7.04	6.48	0.56
500	21.09	20.96	0.13	15.79	16.19	-0.40	5.30	4.77	0.53
600	19.49	19.36	0.13	15.12	15.48	-0.36	4.37	3.88	0.49
700	17.95	17.82	0.13	14.41	14.75	-0.34	3.54	3.07	0.47
800	16.77	16.65	0.12	13.83	14.14	-0.31	2.94	2.51	0.43
900	15.77	15.64	0.13	13.28	13.58	-0.30	2.49	2.06	0.43
1000	14.91	14.79	0.12	12.77	13.04	-0.27	2.14	1.75	0.39
1100	14.20	14.07	0.13	12.28	12.53	-0.25	1.92	1.54	0.38
1200	13.57	13.45	0.12	11.83	12.05	-0.22	1.74	1.40	0.34
1300	13.03	12.92	0.11	11.44	11.64	-0.20	1.59	1.28	0.31
1400	12.59	12.49	0.10	11.12	11.29	-0.17	1.47	1.20	0.27
1500	12.18	12.09	0.09	10.86	10.99	-0.13	1.32	1.10	0.22
1600	11.82	11.74	0.08	10.64	10.73	-0.09	1.18	1.01	0.17
1700	11.54	11.46	0.08	10.43	10.50	-0.07	1.11	0.96	0.15
1800	11.32	11.24	0.08	10.28	10.34	-0.06	1.04	0.90	0.14
1900	11.06	10.98	0.08	10.10	10.16	-0.06	0.96	0.82	0.14
2000	10.85	10.77	0.08	9.97	10.02	-0.05	0.88	0.75	0.13

Finally there does not exist a "standard" near infrared photometric system and this must be kept in mind whenever results from two different instruments are compared.

## References

- Bessell, M.S. & Brett, J.M. 1988, PASP, 100, 1134  
 Burgasser, A.J. et al. 2001, preprint (astro-ph/0108452)  
 Fegley, B. & Lodders, K. 1996, ApJ, 472, L37  
 Gelino, C., Marley, M., Holtzman, J., Ackerman, A., & Lodders, K. 2001, in preparation  
 Hawarden, T.G., Leggett, S.K., Letawsky, M.B., Ballantyne, D.R. & Casali, M.M. 2001, preprint (astro-ph/0102287)  
 Kirkpatrick, J.D. et al. 1999, ApJ, 519, 802  
 Leggett, S.K., Allard, F., Geballe, T.R., Hauschildt, P.H. & Schweitzer, A. 2001a, ApJ, 548, 908  
 Leggett, S.K. et al. 2001b, preprint (astro-ph/0108435)  
 Marley, M.S., Seager, S., Saumon, D., Lodders, K., Ackerman, A.S. & Freedman, R. 2001, preprint (astro-ph/0105438)  
 Noll, K.S., Geballe, T.R., Leggett S.K. & Marley, M.S. 2000, ApJ, 541, L75